https://doi.org/10.5194/egusphere-2026-3332
Preprint. Discussion started: 24 June 2026

Fine-scale Thermohaline Stratification in the Near-Surface Layer Under Weak Wind Conditions with Indications of Salt Fingering

Lisa Deyle[1], Grete Boskamp[2], Jens Meyerjürgens[3], Lars Umlauf[2], Thomas H. Badewien[1]

[1]Carl von Ossietzky Universität Oldenburg, Institute for Chemistry and Biology of the Marine Environment (ICBM), Center for Marine Sensors (ZfMars), Wilhelmshaven, 26382, Germany
[2]Leibniz-Institute for Baltic Sea Research Warnemünde (IOW), Rostock, 18119, Germany
[3]German Aerospace Center (DLR), Institute for the Protection of Maritime Infrastructures, Bremerhaven, 27572, Germany

Correspondence to: Lisa Deyle (lisa.deyle@uni-oldenburg.de)

Abstract. The near-surface ocean regulates air–sea exchange of heat, momentum, and gases, while its fine-scale thermohaline structure remains poorly characterized, particularly under weak wind conditions in tidally influenced shelf seas. High-resolution Lagrangian observations of temperature and salinity in the upper two meters of the German Bight (North Sea) are presented, acquired during a period of weak winds and strong solar radiation. Two minimally invasive Lagrangian surface drifters equipped with a vertical sensor chain enabled continuous measurements within the same water mass, avoiding ship-induced disturbances and resolving the temporal evolution of near-surface stratification in a tidally energetic environment. During the calm period, a pronounced diurnal warm layer developed, with temperature differences of up to 2.5 °C over less than two meters. Concurrently, a distinct salinity anomaly emerged, characterized by higher salinity at 0.55 m compared to 1.75 m depth. Despite these pronounced thermohaline gradients, the water column remained statically stable throughout the observation period, as indicated by the density structure and consistently positive buoyancy frequencies.

Temperature and salinity exhibited variability on timescales of seconds to minutes, indicating the presence of fine-scale processes such as shear-induced interleaving and intermittent vertical motions operating within an otherwise stable near-surface layer. Diagnostics based on the Turner angle and density ratio further suggest conditions favorable for salt-finger-type double-diffusive processes during the calm phase. A comparison with a one-dimensional water column turbulence model shows that while the model reproduces the bulk evolution of the diurnal warm layer, it does not capture the observed fine-scale thermohaline variability.

These observations demonstrate that the near-surface layer in tidally influenced shelf seas can exhibit complex and rapidly evolving thermohaline structures under weak wind conditions and high solar radiation. The results underscore the importance of high-resolution Lagrangian measurements for characterizing near-surface processes and for improving the representation of air–sea exchange with fine-scale processes in coastal and shelf-sea environments.

https://doi.org/10.5194/egusphere-2026-3332
Preprint. Discussion started: 24 June 2026

1 Introduction

The near-surface layer (NSL) is the interface between the ocean and the atmosphere and is crucial for the exchange of heat, momentum, particles, and gases (Cunliffe et al., 2013; Wurl et al., 2016). These exchange processes not only influence the local dynamics of the surface ocean, but also have direct implications for the global climate system. Particularly important is the role of the ocean as a substantial sink for anthropogenic CO_2 emissions. The efficiency of carbon absorption is considerably impacted by the temperature of the sea surface layer (Watson et al., 2020; Yan et al., 2024). This phenomenon can be attributed to the fact that the solubility of gases is influenced by both temperature and salinity (Weiss, 1974). As demonstrated by Watson et al. (2020), solubility and carbon uptake increase when the surface cools down, and decrease when it warms up. Changes in the thermohaline structure of the NSL therefore have an immediate impact on short- and long-term climate regulation.

The temperature and salt distribution in the upper meters of the ocean determine the density in the NSL and govern its stratification. Under moderate to high wind speeds and buoyancy loss, strong turbulent mixing may reduce or disrupt near-surface stratification. However, during periods of low winds and intense surface heating, turbulence is suppressed. This leads to a pronounced, stable temperature stratification that inhibits vertical exchange and thus restricts the transport of gases, heat, and material. The combination of high solar radiation and low wind conditions leads to the evolution of diurnal warm layers (DWLs), whose thickness and intensity are controlled by the balance between surface heating and wind-driven mixing (Price et al., 1986; Schmitt et al., 2024; Yan et al., 2024). Depending on the region and conditions, DWLs can create large temperature differences of several degrees within the first 1–5 m (Dong et al., 2017; Soloviev and Lukas, 1997).

Recent high-resolution studies have provided new insights into the fine-scale structure and temporal evolution of DWLs, revealing pronounced variability on meter and minute scales and highlighting challenges in reproducing these features with one-dimensional turbulence models (Miracca Lage et al., 2025; Witte and Zappa, 2025). While the temperature distribution in the NSL is relatively well documented, the role of salinity under conditions of weak wind and high solar radiation and its interaction with temperature in shaping thermohaline stratification remain less well explored. A better understanding of these processes and the resulting stability characteristics is required for representing them in ocean models applied to seasonal, decadal, and future climate projections.

An additional mechanism that can influence near-surface diapycnal mixing in situations with weak wind forcing are double diffusion processes such as salt fingering or diffusive convection. These arise from different molecular diffusion rates of heat and salt. Bebieva and Timmermans (2016), Schmitt et al. (2005) and St. Laurent and Schmitt (1999) have demonstrated the importance of double diffusion in the ocean interior, where shear-driven mixing is weak. Ashin et al. (2023) shows that double diffusion in the form of salt fingers can also occur during daytime at depths of around 10 m in the diurnal thermocline when shear-driven turbulence is strongly suppressed. However, there is a paucity of knowledge regarding their occurrence within the highly dynamic NSL. In particular, the question of whether salt fingers or other double-diffusive instabilities can occur in the first few meters under weak-wind conditions, and how they might interact with DWL evolution, remains largely unresolved.

https://doi.org/10.5194/egusphere-2026-3332
Preprint. Discussion started: 24 June 2026

One reason for these gaps in knowledge lies in the methodological challenge of observing DWLs and near-surface stratification, especially in tide-dominated coastal regions such as the North Sea, where strong horizontal currents make it more difficult to observe a consistent water mass. Furthermore, ship-based observations may disturb the delicate near-surface structure. As a result, recent studies have increasingly relied on autonomous Lagrangian observing platforms, including gliders and surface drifters, to investigate DWL evolution and near-surface processes (Miracca Lage et al., 2025; Witte and Zappa, 2025). This study combines high-resolution temperature and salinity measurements in the first two meters of a tidally influenced coastal region. The use of Lagrangian surface drifters with a sensor chain makes it possible to track an undisturbed water mass over several hours, while recording the temporal development of thermohaline stratification. This approach allows us to investigate:

(1) how temperature and salinity stratification evolve within the NSL during the formation of a DWL,

(2) what contribution thermohaline variability makes to stratification and exchange, and

(3) whether the observed thermohaline structure provides indications of double-diffusive processes in the first two meters.

In addition, the observed development of the DWL is compared with results from the General Ocean Turbulence Model (GOTM) (Umlauf et al., 2005), which we use to obtain a high-resolution numerical representation of the NSL. This model comparison illustrates to what extent a one-dimensional water-column model can reproduce the bulk evolution of the NSL, while highlighting its limitations in capturing short-lived and strongly pronounced fine-scale structures that involve three-dimensional processes.

Together, the observations and model simulations provide a framework for investigating the temporal evolution of thermohaline stratification and associated fine-scale processes within the NSL under weak-wind conditions in a tidally influenced shelf sea.

2 Study Site and Methods

2.1 Study Site

As part of this study, a research expedition was carried out in July 2024 in the German Bight of the North Sea near Heligoland (Fig. 1). Field measurements were conducted from two vessels, the Research Vessel (RV) Heincke and the Motor Ship (MS) Fritz Reuter. The study area is located in the southeastern North Sea, a semi-enclosed shelf sea that opens into the North Atlantic via the English Channel in the southwest and the Norwegian Sea in the north. The region near Heligoland is shallow, with a water depth of 20–40 m, due to its proximity to the coast (Fig. 1). The circulation in the study area is dominated by semidiurnal tidal dynamics. The M_2 tide with a period of 12.42 h provides a good first approximation for representing tidal motion, noting the tidal currents are also slightly affected by the shallow water tides M_4 and M_6 (Deyle et al., 2024). The currents in the region are also influenced by the prevailing, mostly westerly winds (Becker et al., 1999; Otto et al., 1990).

https://doi.org/10.5194/egusphere-2026-3332
Preprint. Discussion started: 24 June 2026

Currents in the study area typically reach up to 1 m s^{-1} and follow a pronounced tidal ellipse whose major axis is oriented approximately parallel to the coastline (Deyle et al., 2024; Dietrich, 1950).

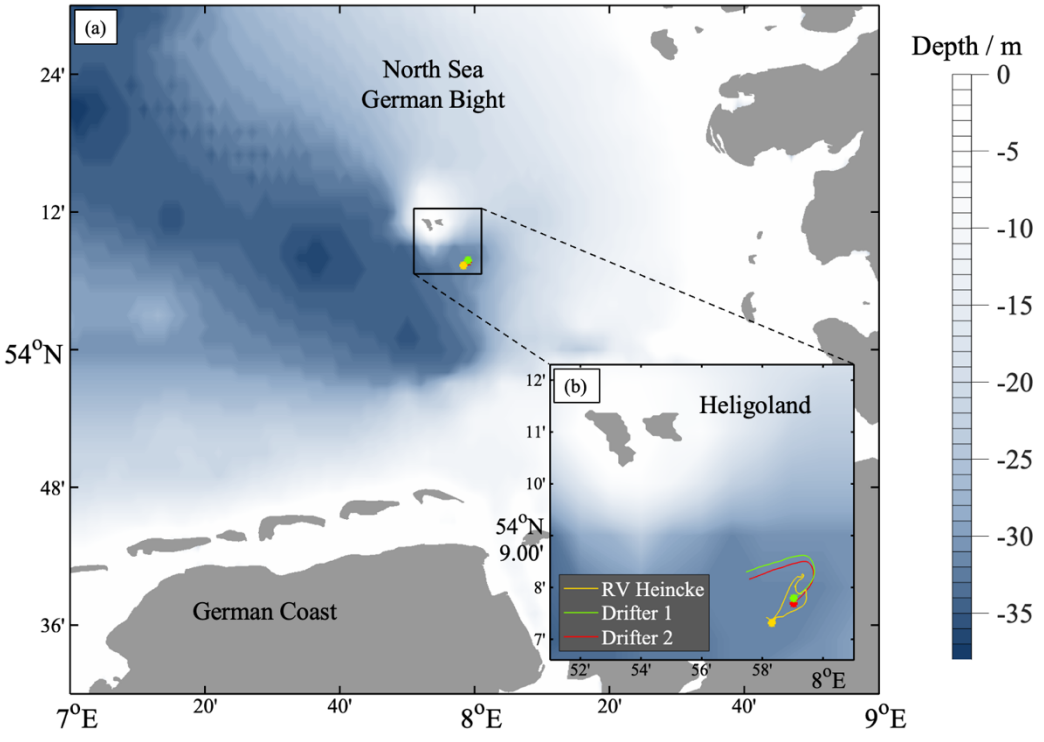

Figure 1: A map of the German Bight (part of the North Sea) and its surrounding area with the German Coast (a), with bathymetry shown in the background. A zoom of the offshore island of Heligoland is shown in (b) with two drifter trajectories (green, red) and the RV Heincke trajectory (yellow) from 21 July 2024. The colored dots represent the starting points of the deployment.

2.2 Meteorological data

The meteorological forcing data were recorded on board RV Heincke using a weather station operated by the German Weather Service (DWD). The station continuously measured air temperature, wind, humidity, and air pressure while the vessel remained within a distance of 2.2 km from the Lagrangian surface drifters presented in Sect. 2.3 (Fig. 1b). Wind speed and wind direction were recorded at a height of 28 m above sea level, relative humidity and air temperature at a height of 18 m, and air pressure at a height of 6 m. At the same time, sea surface conductivity and temperature at a water depth of 3 m were recorded using a thermosalinograph with SBE 21 and SBE 38 sensors from Sea-Bird Scientific (USA). Downward global shortwave radiation and downward longwave radiation in W m^{-2} were recorded at a height of 15.5 m using a pyranometer and a pyrgeometer.

https://doi.org/10.5194/egusphere-2026-3332
Preprint. Discussion started: 24 June 2026

The turbulent momentum flux, the sensible and latent heat fluxes, and the net surface heat flux were calculated from these meteorological data using the COARE bulk algorithm (version 3.6: coare36vnWarm), including cool-skin and warm-layer corrections (Edson et al., 2013; Fairall et al., 1996, 2003).

2.3 Lagrangian Drifter Observations and Data Processing

During the campaign, two Lagrangian surface drifters described in Deyle et al. (2024) and Meyerjürgens et al. (2019) were used (Fig. 2). As Lagrangian platforms, the drifters follow the near-surface water motion, allowing observations within a moving water mass over extended periods with minimal disturbance to the surrounding water. The drifters use a GPS satellite tracker (inReach® Messenger from Garmin Ltd.) with high temporal resolution, which transmitted GPS positions at two-minute intervals. The drifters were equipped with four cruciform drag-producing vanes to follow near-surface currents in the upper 0.5 m while minimizing the direct wind-slip effect.

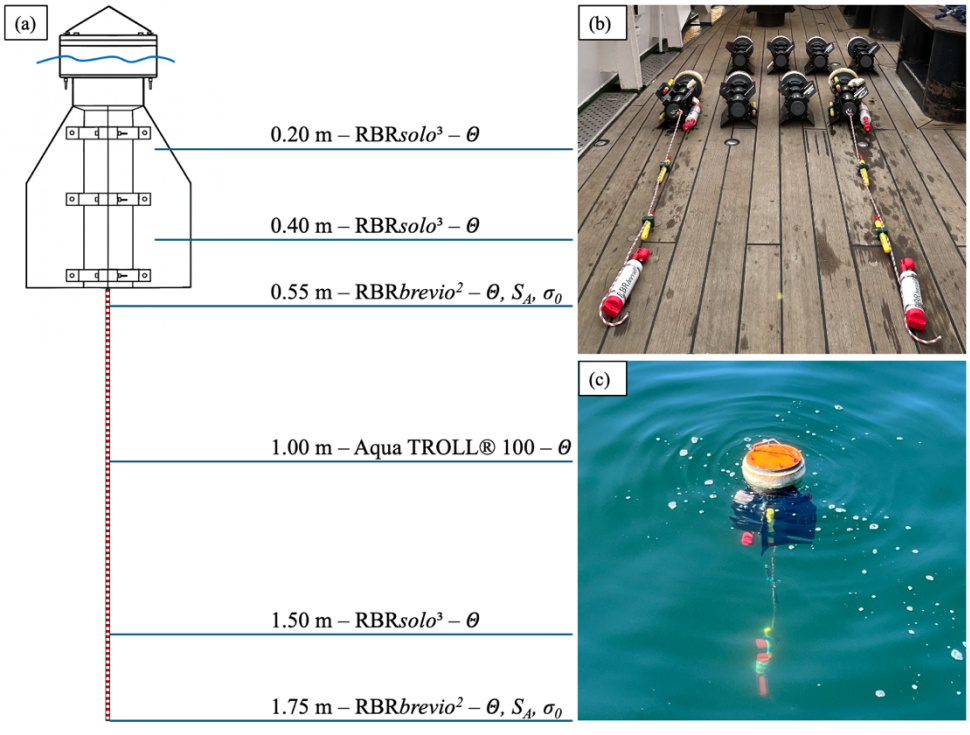

Figure 2: Panel (a) shows a drawing of the surface drifter with sensor chain. The depths of the sensors installed on the drifters are indicated. In addition, the sensor types and parameters available for each depth (conservative temperature Θ, absolute salinity S_A, and potential density anomaly σ_0) are marked. Panel (b) presents a photo of the drifters with installed temperature and CTD sensors. The floating behavior of the drifter with sensor chain during a deployment is shown in panel (c).

https://doi.org/10.5194/egusphere-2026-3332
Preprint. Discussion started: 24 June 2026

In addition, the drifters were equipped with short (down to 1.75 m depth) instrument chains including temperature and lightweight CTD (conductivity, temperature, depth) sensors (Fig. 2). The in-situ temperature was recorded at six different depths within the NSL (Fig. 2a), using RBR*solo*³, RBR*brevio*³ and Aqua TROLL® 100 sensors. Conservative temperature Θ was calculated from in-situ temperature according to the Thermodynamic Equation Of Seawater–2010 (TEOS-10) using the Gibbs Seawater (GSW) Oceanographic Toolbox (McDougall and Barker, 2011).

The RBR sensors measure at a frequency of 2 Hz and the TROLL sensors at 1 min^{-1}. The RBR sensors were calibrated to a measurement uncertainty of ± 0.002 °C, whereas the TROLL sensors have a measurement uncertainty of ± 0.1 °C. An additional offset correction was performed on the TROLL data, using data segments with completely well-mixed conditions in the sensor range. For the offset correction, the difference between each TROLL sensor and the adjacent high-precision RBR sensors was calculated. The mean value of the difference was calculated, and this offset corrected the TROLL data.

The RBR*brevio*³ sensors were positioned at two different depths, at 0.55 m and 1.75 m (Figs. 2a and 2b). These are CTD sensors that measure in-situ temperature, pressure, and conductivity with a high accuracy of ± 0.003 mS cm^{-1}. Note that the conductivity measurements from the TROLL sensors were not used for this purpose, as their accuracy is insufficient to resolve the small salinity differences within the NSL.

Outliers were removed from the raw in-situ temperature and conductivity data using a Hampel median filter. For each data point, the filter calculates the local median within a window of 180 surrounding data points (90 points on each side), corresponding to approximately 90.5 s at a sampling rate of 2 Hz, and estimates the local standard deviation from the median absolute deviation (MAD). Measurement values that deviated by more than three local standard deviations from the median were identified as outliers and removed from the time series (set to NaN). Subsequently, the raw conductivity and temperature data were smoothed using a second-order Butterworth low-pass filter with a cutoff period of 30 s. The filtering was phase-neutral, so that temporal structures in the time series were not shifted. The aim of the filtering was to suppress high-frequency variability and small-scale sensor noise.

From these data, in addition to conservative temperature Θ, absolute salinity S_A, and potential density anomaly σ_0 were calculated in accordance with the TEOS-10 framework for the thermodynamics of seawater, as implemented in the GSW Oceanographic Toolbox (McDougall and Barker, 2011). Similarly, the (square of the) buoyancy frequency N^2 between the two CTD sensors was computed based on the TEOS-10 framework to assess the static stability of the NSL (> 0 corresponds to statically stable stratification) at a midpoint depth of 1.15 m.

https://doi.org/10.5194/egusphere-2026-3332
Preprint. Discussion started: 24 June 2026

2.4 Double-Diffusive Stability Diagnostics

To characterize double-diffusive regimes in the NSL, the Turner angle Tu was used as a diagnostic parameter describing the relative thermal and haline contributions to density stratification (McDougall, 1988; Turner, 1973):

$$Tu = \tan^{-1}\left(\frac{\alpha\Delta\Theta + \beta\Delta S_A}{\alpha\Delta\Theta - \beta\Delta S_A}\right), \quad (1)$$

where α and β denote the thermal expansion and haline contraction coefficients, respectively. Here, $\Delta\Theta$ and ΔS_A represent the vertical differences in conservative temperature Θ and absolute salinity S_A measured by the CTD loggers at 0.55 m and 1.75 m depth (see above). Equivalently, the density ratio R_ρ,

$$R_\rho = \frac{\alpha\Delta\Theta}{\beta\Delta S_A} \quad (2)$$

is frequently used to characterize double-diffusive regimes (McDougall, 1988). While both parameters are derived from the same underlying gradients, the density ratio provides a more direct measure of the relative contributions of the conservative temperature and absolute salinity to the static density stability.

Note that Turner angles in the range $45° < Tu < 90°$, corresponding to $R_\rho > 1$, indicate conditions favorable for salt fingering, whereas values in the range $-90° < Tu < -45°$ ($0 < R_\rho < 1$) are characteristic of diffusive convection (McDougall, 1988; Turner, 1973; You, 2002).

2.5 One-dimensional model description

To support the physical interpretation of our drifter observations, we used the one-dimensional ocean turbulence modelling toolbox GOTM (www.gotm.net, Umlauf et al., 2005). GOTM represents the key hydrodynamic and thermodynamic processes governing vertical mixing in the ocean by solving the one-dimensional transport equations for heat, salt, and momentum. A central component of the model is the parameterization of the turbulent fluxes, which were computed here based on an algebraic second-moment turbulence closure model (Umlauf et al., 2005), solving differential equations for the turbulent kinetic energy and a turbulence length scale as described in detail in Schmitt et al. (2024). However, different from these authors, we did not include a parameterization for Langmuir turbulence, which is likely to have negligible effects in our observations with very small surface-wave activity. As shown by Schmitt et al. (2024), this model reproduces the evolution, structure, and dynamics of DWLs in excellent agreement with Large Eddy Simulations (LES) that served as a benchmark in their study. More recently, Miracca Lage et al. (2025) showed that the same model was able to accurately reproduce glider-based high-resolution observations of stratification and mixing parameters in DWLs in a subtropical region of the South Atlantic Ocean. We therefore believe that GOTM provides a well-tested and reliable tool to complement our drifter-based observations of DWLs in the North Sea. It is important to note, however, that GOTM does not include any parameterization for double-diffusive mixing. This suggest that any observed qualitative differences between GOTM and our field data in the double-diffusive regime, discussed in detail in Section 4 below, provide indications for the actual occurrence of double-diffusive processes not accounted for in the model.

https://doi.org/10.5194/egusphere-2026-3332
Preprint. Discussion started: 24 June 2026

The model was forced with air-sea fluxes calculated using the Coupled Ocean–Atmosphere Response Experiment (COARE) bulk algorithm, as described in Sect. 2.2. An important parameter controlling near-surface warming is the shortwave absorption profile. In our simulations, shortwave penetration in the surface layer was represented by a single-exponential decay function, $I(z) = I_0 e^{z/g_1}$, where $I(z)$ is the shortwave irradiance at depth z, I_0 is the surface irradiance and g_1 is the effective e-folding depth. Because direct optical measurements were not available, we determined g_1 by comparison to the observed thermal structure, resulting in g_1 = 0.6 m.

3 Results

In the following, the observed meteorological and oceanographical conditions and their influence on the thermohaline structure and dynamics of the NSL are presented using physical-oceanographic diagnostics. The measurements took place on 21 July 2024, which included a period with unusually low wind speeds (less than 3 m s^{-1}) and strong solar insulation, followed by an abrupt increase in cloud cover and wind speeds above 10 m s^{-1} (Fig. 4). Optical recordings showed that the sea was very calm during the initial period and showed no wave motion (Fig. S1). Even small capillary waves were suppressed, resulting in a visibly smoother and lighter surface than the surrounding water. Similarly, organic material, foam, and organisms such as jellyfish could be visually identified during the day (Fig. S2).

This situation allowed us to investigate the evolution of DWLs in a low-energy regime that is not well explored, to study DWL destruction by a sudden change in the surface forcing, and to evaluate the representation of these processes in a one-dimension turbulence model.

3.1 Drifter Trajectory and Wind-Slip Characteristics

The trajectories of the Lagrangian drifters (green, red) and RV Heincke (yellow) during and after calm wind conditions and high solar radiation are shown in Fig. 1b. The colored dots represent the starting positions of the drifter deployments. The surface drifters were always within a maximum distance of 2.2 km from RV Heincke to ensure that the meteorological data measured on RV Heincke closely represent the conditions at the drifter locations.

The Lagrangian surface drifters move with the near-surface currents in the upper 0.5 m. In the North Sea near Heligoland, under low wind conditions, the surface current is dominated by the semidiurnal M_2 tide and the shallow water overtides M_4 and M_6, resulting in an elliptical movement (Deyle et al., 2024; Meyerjürgens et al., 2019). This is clearly visible in Fig. 3, which shows the trajectory of Drifter 1 on 21 July together with the corresponding flow velocity (color-coded). Initially, the drifter moves northeast during the late flood phase at comparatively low velocities, as high tide occurred at 10:50 UTC. Afterwards the drifter changes the direction to the west and then speeds up again with the ebb surface current.

Meyerjürgens et al. (2019) showed that this type of drifters experiences a low wind slip of 0.27 % of the wind speed. The wind slip denotes the small velocity of the drifter relative to the surrounding surface water caused by direct wind drag on the exposed float. In Fig. 3, the wind-slip-corrected drifter positions are shown as dashed lines, representing the estimated pure surface

https://doi.org/10.5194/egusphere-2026-3332
Preprint. Discussion started: 24 June 2026

current pathway in the absence of direct wind slip. Until 12:19 UTC (gray-shaded region), the deviation between the wind-slip-corrected current path and the original drifter trajectory remains small (see Fig. 3 lower panel), reaching a maximum of 17.7 m at 12:18 UTC. This is due to persistently low wind speeds below 3 m s^{-1} for the first observation period. Under these conditions, the drifter largely remains within the same near-surface water mass, thus representing a Lagrangian view of the fluid motion.

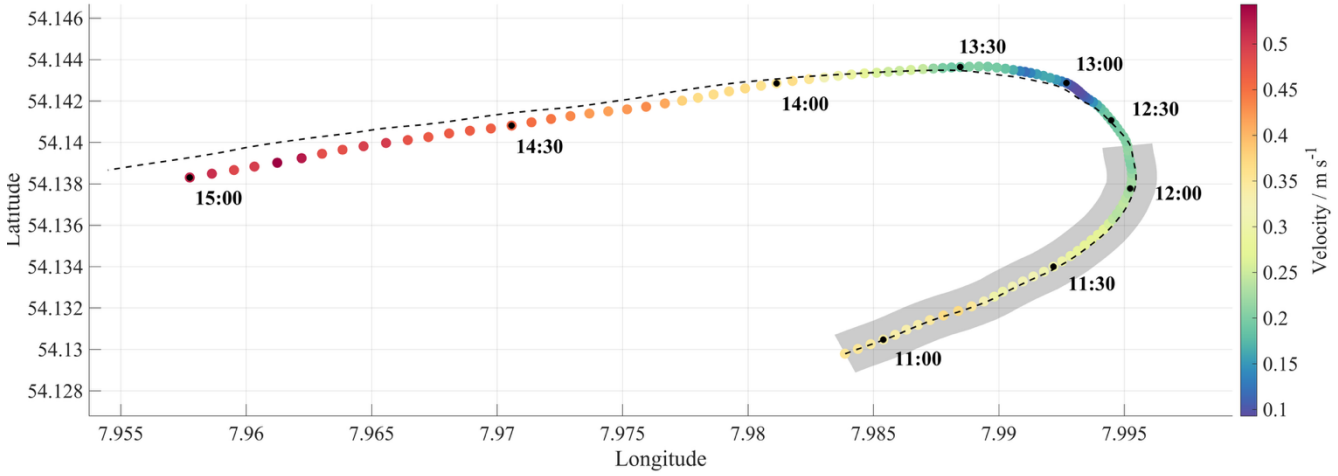

Time / UTC	11:00	11:30	12:00	12:30	13:00	13:30	14:00	14:30	15:00
Wind direction	↖	↖	↑	→	→	↘	↘	↘	↘
Wind speed / m s^{-1}	1.9	1.7	1.3	4.9	6.2	12.8	10.5	10.5	8.9
Wind-slip-induced displacement / m	2.3	10.0	15.2	16.3	29.5	83.2	132.2	177.5	216.4

Figure 3: Drifter trajectory of Drifter 1 from 21 July 2024 is shown, with color representing the flow velocity of the drifter in m s^{-1}. The trajectory minus the wind slip (0.27% of the wind speed) is shown in dashed lines, representing the estimated surface-current path without direct aerodynamic wind drag. The first measurement period, during calm wind conditions, is shown in gray. The lower panel presents the half-hourly mean wind direction (arrows), the mean wind speed in m s^{-1}, and the instantaneous distance between the original and wind-slip-corrected drifter trajectories in m (wind-slip-induced displacement).

3.2 Temporal Evolution of Diurnal Near-Surface Temperature Stratification

The temporal evolution of temperature during the period shown in Fig. 3 is presented in Fig. 4a. Data from the six available temperature sensors of Drifter 1 were linearly interpolated onto a finer vertical grid for plotting (instrument depths are indicated). A corresponding temperature plot for Drifter 2 is provided in Fig. S3 and shows a similar overall evolution. Based on the wind conditions (Fig. 4b), three periods can be distinguished, which are represented by three different background colors in Fig. 4. The first period (purple) runs from approximately 10:50–12:19 UTC. This period is characterized by weak winds of less than 3 m s^{-1} and the evolution of a thin DWL, with a maximum temperature of 21.3 °C at the surface and

https://doi.org/10.5194/egusphere-2026-3332
Preprint. Discussion started: 24 June 2026

18.6 °C at the location of the deepest sensor at 1.75 m depth. Interesting is the pronounced short-term temperature variability during this period, which will be discussed in more detail below.

The second period (red) begins with an increase in wind speed to approximately 5–6 m s^{-1}. The temperature stratification begins to break down shortly afterwards. A clear response throughout the entire observed water column becomes apparent at around 12:40–12:45 UTC, when the previously strong temperature stratification weakens abruptly throughout the observed water column. We attribute this offset to the small-scale variability in the wind field between the drifter (temperature measurements) and RV Heincke (wind measurements), as well as to a temporal delay between the increase in wind speed and the resulting onset of enhanced vertical mixing. In the third period, the wind increases further after 13:00 UTC, reaching speeds of over 11 m s^{-1}, and the water column continues to mix. From around 13:23 UTC onwards, nearly identical temperatures are observed across the entire sensor range. The near-surface region is well mixed across the entire sensor range during this final period of our observations.

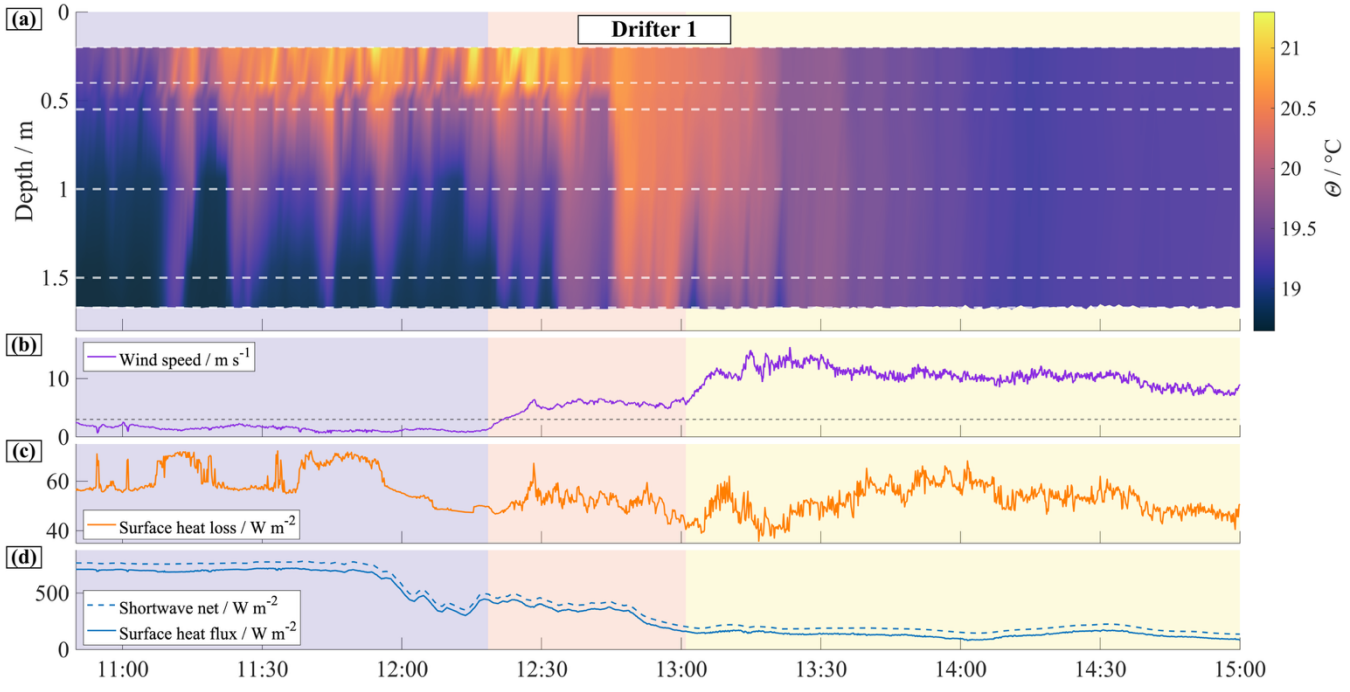

Figure 4: Panel (a) shows the conservative temperature values of Drifter 1 with sensor chain from 21 July 2024. The temperature values are interpolated over depth and time. The dashed white lines indicate the average depth positions of the sensors. Panel (b) shows the wind speed in m s^{-1} measured with RV Heincke. Panel (c) presents the surface heat loss in W m^{-2} (latent heat flux + sensible heat flux + net longwave radiation) and panel (d) the net shortwave radiation and surface heat flux in W m^{-2}, calculated using the COARE bulk algorithm. The background colors (violet, red and yellow) indicate three different periods of wind (b).

The surface heat loss (Fig. 4c) shows only moderate variability throughout the observation period, ranging between approximately 40 and 70 W m^{-2}, with a slight decrease after approximately 11:50 UTC. In contrast, net shortwave radiation and surface heat flux (Fig. 4d) decrease markedly after 11:50 UTC, consistent with increasing cloud cover. Net shortwave

https://doi.org/10.5194/egusphere-2026-3332
Preprint. Discussion started: 24 June 2026

radiation decreases from peak values of about 780 W m^{-2} to below 200 W m^{-2}, while the surface heat flux drops from approximately 720 W m^{-2} to below 150 W m^{-2}. The resulting reduction in the stabilizing effect of solar heating, combined with increasing wind speeds, promotes the erosion of the shallow temperature stratification and contributes to the breakdown of the DWL.

3.3 Comparison of GOTM-Simulated and Observed DWLs

The numerical simulation with the one-dimension ocean turbulence model described in Section 2.5 was started at 10:00 UTC on 21 July 2024, i.e. slightly less than one hour before the start of the drifter deployments. Due to the shallowness of the DWL (less than 0.5 m, initially), this short spin-up period turned out to be sufficient to yield a stable, well-developed DWL that was not sensitive to the changes in the small variations in the starting point of the simulation. The simulation was initialized with the (linearly interpolated) temperatures and salinities observed by the drifting instrument chains directly after their deployment (10:50 UTC) in the upper 1.75 m of the water column, combined with a full-depth CTD profile that was obtained nearby right after the drifter deployment (11:08 UTC). The model was forced with heat and momentum fluxes derived from the ship's meteorological data as described in more detail in Section 2.2 above. Due to the close proximity between the ship and the drifters (see above), we believe that the observed meteorological forcing is representative also at the drifter locations. The simulation was carried out with a vertical resolution of 0.05 m and a time step of 5 s, which were found sufficiently small to yield fully converged numerical solutions. We interpret these simulations as representing the purely wind driven effects on the Langrangian drifters, thus ignoring the effects of the tides, which are unlikely to provide any significant near-surface shear and therefore do not contribute to near-surface mixing.

Fig. 5a, b shows that during the initial phase (the three phases are separated by the dashed white lines in the figure), the model predicts the evolution of a shallow DWL with a turbulent, well-mixed near-surface region of approximately 0.3 m depth above a non-turbulent deeper layer. The heating observed below this turbulent near-surface region (Fig. 5a) therefore cannot be due to the downward mixing of heat but has to be attributed to the penetrative short-wave radiation shown in Fig. 5c. Comparison with Fig. 4a suggest that, during this initial phase, the model reproduces the overall evolution of the observed temperature structure with good accuracy, although simulated near-surface temperatures remain systematically lower than the observations during the calm period. In addition, the model does not reproduce the striking short-term fluctuations in temperature that are especially evident below the well-mixed surface region. Potential explanations for these fluctuations as well as the systematically lower near-surface temperatures will be discussed in the following section.

The model responds to the gradual increase in wind speed and cloud cover during phase 2 with a gradual entrainment of the DWL into the underlying, non-turbulent fluid down to approximately 1 m depth, and finally, with the onset of the strong winds characterizing phase 3, with complete mixing across the entire sensor range (Fig. 5a, b). While the entrainment process in the deeper regions below the sensor range cannot be directly observed due to the lack of data, the gradual cooling seen in both the data (Fig. 4a) and the model (Fig. 5a) are clearly indicative for the entrainment of cold deeper water, overwhelming the ongoing

https://doi.org/10.5194/egusphere-2026-3332
Preprint. Discussion started: 24 June 2026

net surface heating. While the overall evolution of the near-surface region is in good agreement with the observations, the almost instantaneous DWL deepening seen in the data around 12:40-12:45 UTC is not reproduced by the model.

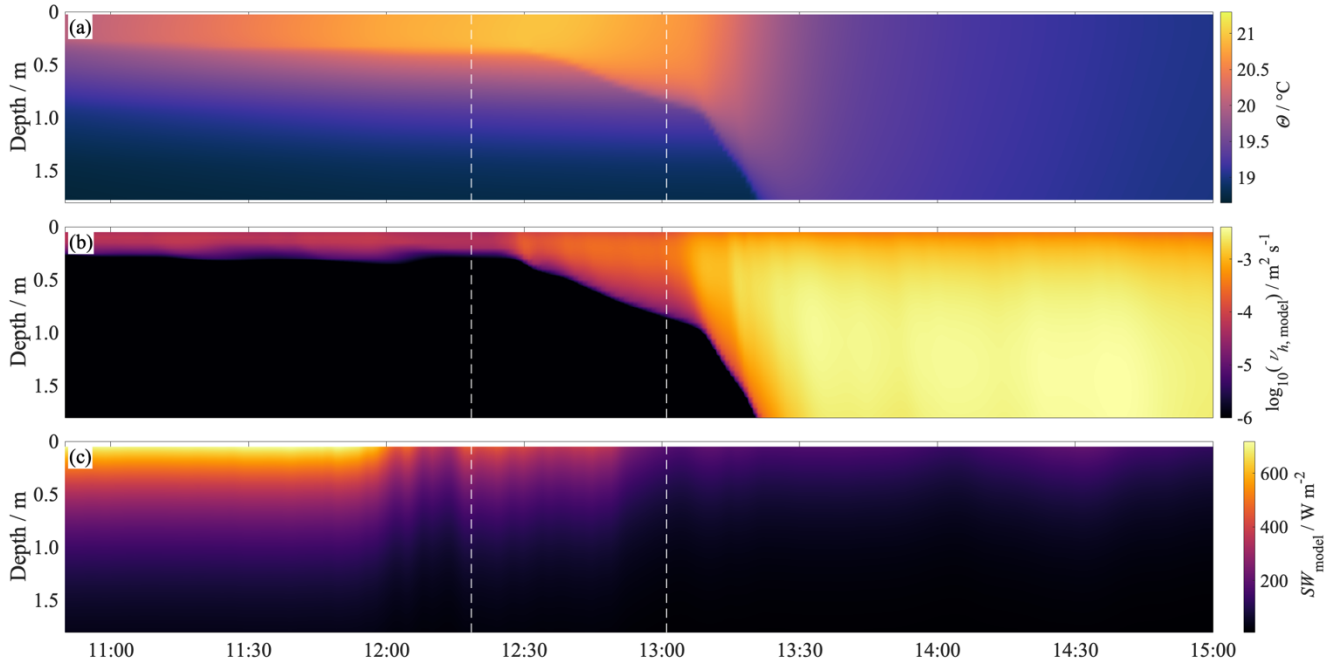

Figure 5: Results from the one-dimensional water column model GOTM, showing (a) conservative temperature, (b) turbulent diffusivity of heat, and (c) penetrating short-wave radiative heat flux, computed from the observed surface short-wave radiative flux and the exponential decay law discussed in Section 2.5. The time period and vertical axis range correspond exactly to those in Fig. 4a. The dashed white lines separate the three wind regimes identified in Fig. 4.

3.4 Thermohaline Stratification of the NSL

Fig. 6 shows stratification parameters for the same period for the two available drifters with two CTD sensors at depths of 0.55 m and 1.75 m. The data in Fig. 6c, d show that, during the first period (purple) and extending into the beginning of the second period (red), the water column is stably stratified throughout the sensor range due to the stable temperature stratification associated with the evolution of the DWLs (Fig. 6e, f). Interestingly, however, our data suggest an inverse (destabilizing) salinity stratification with an average salinity difference of -0.04 g kg^{-1} (-0.02 g kg^{-1} for Drifter 2) and peak values up to -0.18 g kg^{-1} (Fig. 6a, b). The salinity in the upper layer is highly variable over time and may vary strongly within seconds. Both drifters exhibit this inverse salinity stratification throughout the first period, and the signal remains visible into the second period until the onset of enhanced mixing at around 12:45 UTC. In addition, the deeper sensors of both drifters show transient temperature peaks on time scales of minutes that are clearly reflected also in the density records. For Drifter 1, some of these

https://doi.org/10.5194/egusphere-2026-3332
Preprint. Discussion started: 24 June 2026

features are additionally accompanied by lower salinity at depth. These structures persist on time scales of several minutes and indicate the presence of distinct thermohaline variability within the NSL. A potential physical explanation for these short-term features will be examined and discussed in more detail below.

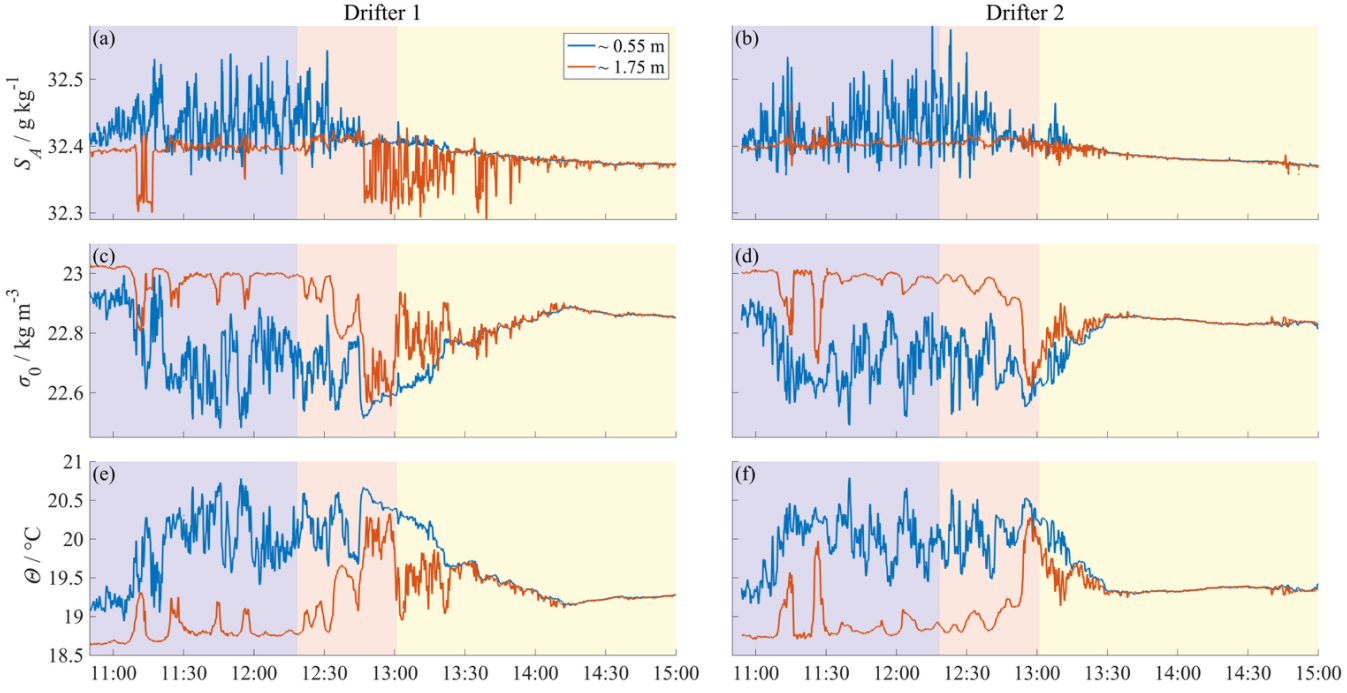

Figure 6: The calculated absolute salinity S_A in g kg^{-1} (a, b), potential density anomaly σ_0 in kg m^{-3} (c, d), and conservative temperature Θ in °C (e, f) over time of the two high-resolution CTD sensors are presented. Panels in the left column (a, c, e) correspond to Drifter 1, while panels in the right column (b, d, f) correspond to Drifter 2. The background colors (violet, red and yellow) mark the analysis periods used throughout the study.

In the second period, temperature and salinity at the two levels converge in response to the increasing wind, and the inverse salinity stratification weakens substantially. For Drifter 2, this transition results in a rapid homogenization of the two sensor levels. In contrast, Drifter 1 continues to exhibit intermittent salinity fluctuations at the deeper sensor during the transition phase, despite the weakening surface salinity anomaly. From approximately 13:50 UTC onward, temperature, salinity, and density at both depths also converge for Drifter 1, indicating complete mixing of the NSL. This general evolution is consistent for both drifters, although short-term differences between the records can be attributed to local small-scale variability along the trajectories.

3.5 Stability and Double-Diffusive Regime

Fig. 7a, b show that the NSL is stably stratified throughout the observation period with a tendency for decreasing stratification in period 2, and a nearly well-mixed NSL in period 3 from around 13:30 UTC onwards.

https://doi.org/10.5194/egusphere-2026-3332
Preprint. Discussion started: 24 June 2026

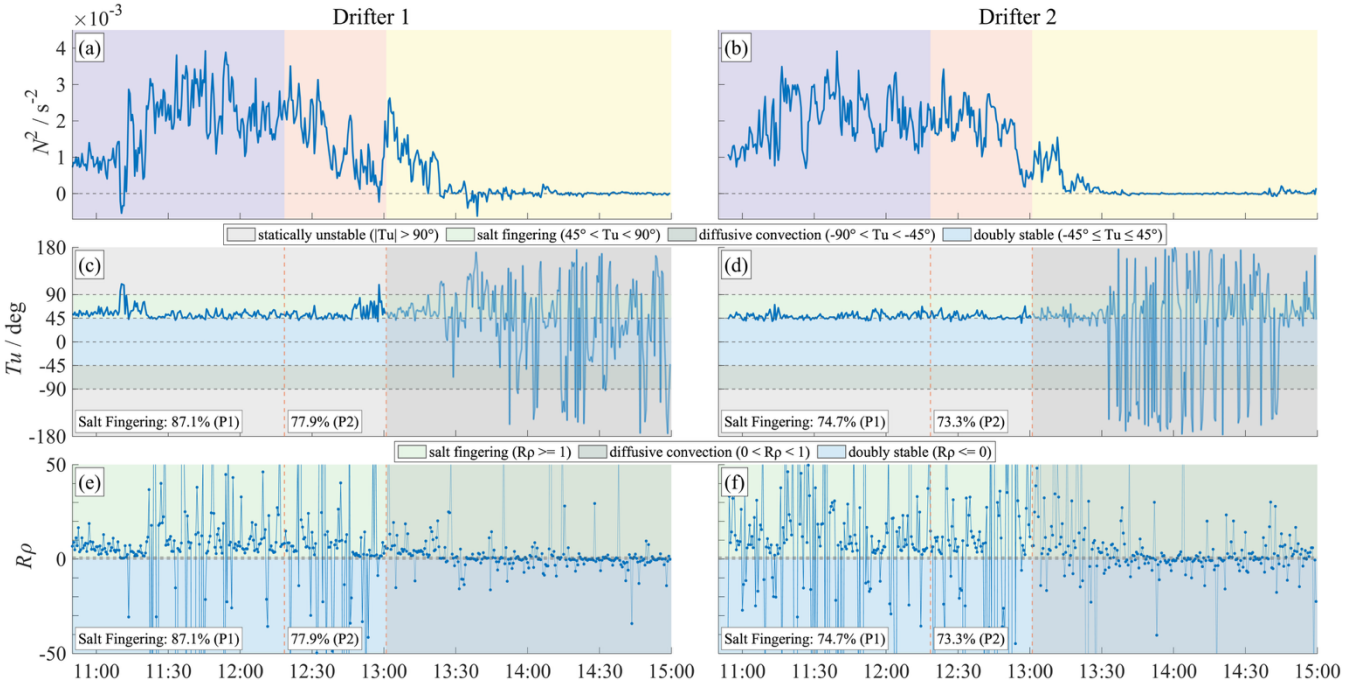

Figure 7: Panels in the left column (a, c, e) correspond to Drifter 1, while panels in the right column (b, d, f) correspond to Drifter 2. The calculated Brunt-Väisälä frequency squared N^2 in rad^2 s^{-2} between the two sensor depths is presented in panels (a, b). Shaded areas mark the analysis periods used throughout the study. In Panel (c, d) the Turner angle *Tu* in deg is shown, and the density ratio R_ρ (unitless) in (e, f). All data were median-averaged over 30-second intervals. The different colors in panel (c-f) distinguish between statically unstable (grey), salt fingering (light green), diffusive convection (dark green), and doubly stable conditions (blue). For transparency, in panel (c-f) the third period is shown but has been shaded out, as the analysis is not typically applied in conditions of high wind and high turbulence.

Statically stable conditions, however, do not preclude the occurrence of double-diffusive instabilities. To investigate the possibility double-diffusive NSL instabilities, the Turner angle *Tu* and density ratio R_ρ were calculated according to Sect. 2.5. Both parameters clearly indicate that the salt fingering form of double diffusion may occur during most of periods 1 and 2 until the start of the third period around 13:01 UTC (Fig. 7b-f). For both drifters, the majority of observations during periods 1 and 2 fall within the salt-fingering regime. For Drifter 1, the corresponding fractions are 87.1 % and 77.9 %, while Drifter 2 shows values of 74.7 % and 73.3 %, respectively. The remaining observations mainly correspond to doubly stable conditions. Both drifters consistently indicate salt-fingering conditions during the formation of the DWL, although the relative occurrence differs slightly between the two records. Starting at 13:01 UTC (third period), the NSL becomes essentially well-mixed and the analysis in terms double-diffusive parameters is not significant any more.

https://doi.org/10.5194/egusphere-2026-3332
Preprint. Discussion started: 24 June 2026

4 Discussion

Our data from small and light-weight (and therefore minimally invasive) drifting platforms allowed us to investigate the dynamics of very shallow DWLs in a low-energy regime that is not typically accessible with conventional instrumentation. The most interesting features discussed in the following include (a) the evolution of extremely shallow DWLs under light-wind conditions with decimeter-scale thickness, significantly thinner than the estimated short-wave light absorption scale, (b) the evolution of inverse salinity stratification near the surface, generating conditions favorable for salt fingering, (c) the abrupt destruction of this near-surface stratification following a sudden increase in wind speed and cloud cover, both favoring turbulence, (d) a strong short-term variability of near-surface salinity and temperature that could not be reproduced by our model. In the following, we discuss the mechanisms that may have contributed to these observations, including the role of double-diffusive processes, frontal variability, and natural surface slicks, and assess the extent to which a state-of-the-art turbulence model is able to represent the observed data set of the NSL.

4.1 Development of the DWL Under Weak Wind Conditions

A key component of DWL dynamics is the existence of a diurnal jet, resulting from the trapping of momentum in the stratified near-surface region (Price et al., 1986). The vertical shear associated with the diurnal jet has been identified as the main energy source for DWL turbulence and DWL deepening by entrainment (Miracca Lage et al., 2025; Schmitt et al., 2024). However, as pointed out by Schmitt et al. (2024), thin DWLs forced by very weak winds and strong solar insulation may enter a regime in which molecular effects (low Reynolds number) become relevant. The performance of essentially all existing ocean turbulence models in this low-energy regime is uncertain at the moment.

Our simulations show, however, that the second-moment closure model in GOTM is able to reproduce to the key parameters of the very thin DWLs found in our study with sufficient accuracy. Different from most previous DWL studies, in which heat is vertically distributed across the entire thickness of the DWL by turbulent mixing, in our data the region with active shear-driven turbulence is significantly thinner than the short-wave penetration depth. This implies a significant heating signal also below the turbulent near-surface part of the DWL, as reproduced by our model.

A number of important aspects of our data set, however, could not be reproduced by the model. These include the extremely rapid (time scale of minutes) destruction of near-surface stratification during a period with a sudden increase in wind stress and insolation loss (see Fig. 4 at around 12:40 UTC). Different from the observations, our simulations instead predict a gradual DWL entrainment over a period of 0.5–1 hour. Similar discrepancies between observations and one-dimensional model simulations have recently been reported by Witte and Zappa (2025), who noted that none of their models (including a GOTM configuration similar to ours) was able to reproduce the rapid deepening of DWL they observed in their DWL data in response to a sudden insolation loss. Witte and Zappa (2025) speculate that the rapid destruction of near-surface stratification results from the sudden overturning of the entire near-surface region as part of a large-scale shear instability in the marginally stable NSL. A similar process may also have contributed to the rapid breakdown of stratification observed in our data set.

https://doi.org/10.5194/egusphere-2026-3332
Preprint. Discussion started: 24 June 2026

Other important aspects that our one-dimensional turbulence model could not reproduce include the pronounced short-term variability of temperature and salinity inside and below the DWL. While the model captured the overall evolution of the DWL and the wind-driven mixing during periods of stronger forcing, it failed to reproduce the fine-scale thermohaline variability observed under weak-wind conditions. In addition, the model did not generate the observed inverse salinity stratification, leading to conditions favorable for salt fingering. We will discuss these aspects in the following.

4.2 Origin and Persistence of the NSL Salinity Inversion

An important feature in our data is the inverse salinity stratification in the NSL (Fig. 6a, b), creating conditions favorable for salt fingering. Given surface heat fluxes reaching up to 720 W m^{-2} (Fig. 4c), it is tempting to assume evaporation as a potential driver of the increased near-surface salinity. A freshwater loss of approximately 0.5–3.0 mm due to evaporation would be required to produce the observed salinity increase of 0.03–0.18 g kg^{-1} across a layer extending from the surface down to the depth of our first CTD sensor at 0.55 m (see Supplement S1-S3). The actual evaporation rates, estimated using the COARE bulk algorithm, are, however, much smaller than this value (see S4). During the time interval from 10:50 to 12:30 UTC, when the salinity anomaly is observed, the cumulative evaporation from COARE amounts to only 0.02 mm (Fig. S4), while, over the full period from 10:50 to 15:00 UTC, it increases to 0.12 mm. These values are 1–2 orders of magnitude too small to explain the observed salinity increase, demonstrating that evaporation alone is insufficient to explain the observations.

The persistence of the anomaly therefore suggests that additional mechanisms contributed to maintenance of the inverse salinity stratification the NSL. The most plausible explanation seems to be near-surface differential advection of salinity associated with the diurnal jet. In the vicinity of lateral salinity gradients, the vertically sheared jet will induce vertical salinity stratification by the differential advection. We don't have any observations directly supporting the existence of lateral salinity gradients in our study area. It is well-known, however, that the German Bight is a region strongly affected by freshwater runoff, which is clearly evident also in our data from the reduced salinities around 32.3–32.6 g kg^{-1} (Fig. 6a, b), significantly smaller than oceanic values. Previous studies have shown that freshwater runoff and tidal dynamics generate pronounced frontal and filamentary structures in the German Bight, associated with strong horizontal salinity gradients (Albinus et al., 2025; Meyerjürgens et al., 2020; Ricker et al., 2021). It is therefore very likely that the horizontal salinity gradients are ubiquitous in this region.

4.3 Fine-Scale Thermohaline Variability and Indications of Double Diffusion

To assess the dynamical context of the observed inverse salinity anomaly, the vertical density structure of the NSL was examined. Despite the inverse salinity stratification, the NSL remained statically stable throughout periods 1 and 2, as indicated by positive values of the buoyancy frequency N^2 (Fig. 7a, b). However, the observed 'temperature fingers' (Fig. 4a), some extending down to about 1.75 m, together with strong salinity fluctuations (Fig. 6a, b), indicate pronounced fine-scale structure within the otherwise stable NSL. Since statically stable conditions do not preclude the occurrence of double-diffusive instabilities, the potential role of such processes was examined. Analysis of the Turner angle and the density ratio indicates

https://doi.org/10.5194/egusphere-2026-3332
Preprint. Discussion started: 24 June 2026

conditions consistent with the formation of salt fingers (Fig. 7c-f), which are known to develop preferentially under weakly turbulent conditions (Ashin et al., 2023; Schmitt et al., 2005).

The simultaneous presence of strong thermal stratification, persistent inverse salinity gradients, and fine-scale thermohaline variability persisting on timescales of several tens of seconds to minutes supports the interpretation that double-diffusive processes may have contributed to the observed thermohaline structure within the NSL. Furthermore, the weak-wind conditions and the very shallow DWL observed during period 1 may have favored the relative importance of molecular diffusion processes, which are essential for the development of double-diffusive instabilities.

In addition to the rapid short-term fluctuations, both drifters also exhibited thermohaline structures that persisted on timescales of several minutes. These events were characterized by slightly elevated temperatures and reduced densities at the deeper sensor and, in some cases, additionally by lower salinity. Since the drifters primarily followed the motion of the NSL, these deeper anomalies may reflect intermittent interaction of the lower sensor with adjacent water masses exhibiting different thermohaline properties. As wind speeds were very low during this period, it is unlikely that these structures were generated by direct disturbances caused by the drifters themselves.

As discussed in Sect. 4.2, frontal and filamentary structures associated with freshwater influence are common in the German Bight (Albinus et al., 2025; Meyerjürgens et al., 2020; Ricker et al., 2021). The observed variability may therefore reflect the sampling of small-scale thermohaline structures originating from such frontal features.

In contrast, slower large-scale advection alone cannot account for the rapid fluctuations observed in the NSL. Furthermore, the observed structures cannot be attributed to free or wind-driven convection, which can therefore be ruled out as the primary mechanism.

It should be noted, however, that no direct measurements of turbulence intensity or dissipation rates (ε, χ) are available. The assessment of turbulence conditions therefore relies on indirect indicators such as static stability, stratification strength, and the temporal persistence of the observed structures. A more quantitative evaluation of the role of weak turbulence and double-diffusive processes would require additional high-resolution turbulence measurements within the uppermost meters of the water column, which is technically challenging and was therefore not available during this study.

4.4 Potential Influence of Surface Slicks on Near-Surface Stratification

An open question remains as to whether diurnal warming alone under low-turbulence conditions is sufficient to generate the observed stratification and potential salt fingering. Previous studies have shown that the accumulation of organic material can form a biofilm-like surface layer associated with natural slicks, suppressing capillary waves and modifying surface properties (Gade et al., 2006; Laxague et al., 2024; Watson et al., 1997; Wurl et al., 2016). Such an effect was visible on 21 July 2024, and organisms such as jellyfish were observed concurrently, consistent with observations reported by Gallardo et al. (2021). Reports by Foroughan et al. (2022) and Gallardo et al. (2021) also confirm the occurrence of natural slicks at wind speeds below 5 m s^{-1}, which correspond to wind speeds on 21 July 2024.

https://doi.org/10.5194/egusphere-2026-3332
Preprint. Discussion started: 24 June 2026

Slicks can amplify existing surface heat-flux regimes. At night, slick-covered areas appear cooler because surfactants suppress near-surface turbulence and surface renewal, allowing the cool skin to persist (Marmorino and Smith, 2006). During daytime heating, the same suppression reduces vertical exchange and turbulent heat loss, resulting in warmer surface temperatures within slicks. This mechanism may also help explain the systematically lower near-surface temperatures simulated by GOTM during the calm period, since processes associated with natural slicks are not represented in the model configuration used here. Furthermore, Wurl et al. (2018) report lower salinity within slicks compared to surrounding waters, likely due to reduced air–sea exchange. This suggests that salt-finger processes may be enhanced outside slicks, where evaporation is less suppressed. The suppression of near-surface mixing under such strongly damped surface conditions may have additionally favored the persistence of sharp thermohaline gradients within the NSL.

5 Summary and Conclusion

This study investigated the thermohaline structure and dynamics of the NSL in a tidally influenced shelf sea under conditions of weak winds and strong solar radiation. Using high-resolution Lagrangian surface drifters equipped with a vertical sensor chain, temperature and salinity variability in the upper two meters of the water column could be observed continuously within the same water mass, overcoming many of the observational limitations that typically affect near-surface measurements.

(1) The results demonstrate that strong and highly dynamic thermohaline stratification can develop in the NSL even in a region dominated by tidal currents. Temperature differences of up to 2.5 °C over less than two meters highlight the rapid formation and persistence of a DWL under calm conditions.

(2) Pronounced salinity anomalies were observed, with a more saline layer at approximately 0.55 m overlying fresher water at around 1.75 m depth. A quantitative comparison with evaporation estimates derived from the COARE bulk algorithm shows that evaporation alone is insufficient to explain the magnitude of the observed salinity increase. Despite these anomalies, the water column remained statically stable throughout the calm period, as confirmed by consistently positive buoyancy frequencies.

(3) The high temporal variability of temperature and salinity on timescales of tens of seconds to minutes indicates that small-scale processes play a key role in forming the NSL. The observations indicate pronounced fine-scale thermohaline variability within the statically stable NSL. Diagnostics based on the Turner angle and density ratio further suggest that salt-finger-type double-diffusive processes may contribute to the observed fine-scale structure. In contrast, classical convective or wind-driven mixing can be ruled out as the primary mechanism during the calm phase.

A comparison with the one-dimensional water column model GOTM shows that while the model reproduces the bulk evolution of near-surface warming and subsequent mixing during increasing wind speeds, it does not capture the observed strong warming of the surface and the fine-scale thermohaline variability. Because temperature and salinity gradients in the NSL directly control stratification and vertical exchange, the inability to represent this fine-scale variability may affect estimates of

https://doi.org/10.5194/egusphere-2026-3332
Preprint. Discussion started: 24 June 2026

heat, gas, and material fluxes across the air–sea interface, including the oceanic uptake of atmospheric CO_2. This highlights a limitation of commonly used vertical mixing parameterizations when applied to the NSL under weak wind conditions.

Overall, this study underscores that the NSL exhibits complex and highly dynamic thermohaline structures that are not adequately represented by assumptions of vertical homogeneity in the upper ocean and are often unresolved by conventional observing systems. High-resolution Lagrangian measurements are essential to resolve these processes and to improve the representation of near-surface exchange in observational analyses and numerical models. Given the importance of the NSL for air–sea heat and gas exchange, a more explicit consideration of its fine-scale dynamics is required to better quantify short-term variability and its implications for coastal and shelf-sea systems. Improved understanding and representation of these processes are essential for accurately characterizing air–sea exchange processes in coastal shelf seas, including the exchange of heat and gases across the ocean–atmosphere interface. This is particularly relevant for estimates of air–sea CO_2 exchange and their implications for regional carbon cycling and the global climate system.

Data Availability

The drifter position data and the associated hydrographic measurements have been submitted to PANGAEA and are currently awaiting DOI assignment. All data are available on request from the corresponding author.

Author Contribution

LD performed the data analysis and prepared the first draft of the manuscript. The conceptualization and project administration was done by THB and LD. LD and JM carried out the data acquisition. GB performed the model analysis. LU and THB substantially contributed to the revision and refinement of the manuscript, including the interpretation and discussion of the results. All authors contributed to the critical revision of the article and provided important advice for the improvement of the manuscript.

Competing interests

The authors declare that they have no conflict of interest.

Acknowledgments

The data was collected as part of the project “Biogeochemical processes and Air-sea exchange in the Sea-Surface microlayer” (BASS) grant no. 451574234, funded by the German Research Foundation (DFG). The authors would like to thank all members of the BASS research group for their successful collaboration and support in collecting the drifter data. We would like to thank

https://doi.org/10.5194/egusphere-2026-3332
Preprint. Discussion started: 24 June 2026

the master and crew onboard the MS Fritz Reuter and RV Heincke HE644 for supporting the deployments of the drifters. ChatGPT (OpenAI) was used for text refinement and language polishing,

Funding

This study was carried out within the project BASS "Biogeochemical processes and Air-sea exchange in the Sea-Surface microlayer" (grant no. 451574234) funded by German Research Foundation.

References

Albinus, M., Badewien, T. H., Gassen, L., Wurl, O., and Meyerjürgens, J.: Filamentogenesis and Filamentolysis of a Light Filament: Dynamic Processes in the Near-Surface Ocean Under Tidal Forcing, https://doi.org/10.5194/egusphere-2025-4953, 17 October 2025.

Ashin, K., Girishkumar, M. S., D'Asaro, E., Jofia, J., Sherin, V. R., Sureshkumar, N., and Rao, E. P. R.: Observational evidence of salt finger in the diurnal thermocline, Sci. Rep., 13, 3627, https://doi.org/10.1038/s41598-023-30564-5, 2023.

Bebieva, Y. and Timmermans, M.: An examination of double-diffusive processes in a mesoscale eddy in the Arctic Ocean, J. Geophys. Res. Oceans, 121, 457–475, https://doi.org/10.1002/2015JC011105, 2016.

Becker, G. A., Giese, H., Isert, K., König, P., Langenberg, H., Pohlmann, Th., and Schrum, C.: Mesoscale structures, fluxes and water mass variability in the German Bight as exemplified in the KUSTOS- experiments and numerical models, Dtsch. Hydrogr. Z., 51, 155–179, https://doi.org/10.1007/BF02764173, 1999.

Cunliffe, M., Engel, A., Frka, S., Gašparović, B., Guitart, C., Murrell, J. C., Salter, M., Stolle, C., Upstill-Goddard, R., and Wurl, O.: Sea surface microlayers: A unified physicochemical and biological perspective of the air–ocean interface, Prog. Oceanogr., 109, 104–116, https://doi.org/10.1016/j.pocean.2012.08.004, 2013.

Deyle, L., Badewien, T. H., Wurl, O., and Meyerjürgens, J.: Lagrangian surface drifter observations in the North Sea: an overview of high-resolution tidal dynamics and surface currents, Earth Syst. Sci. Data, 16, 2099–2112, https://doi.org/10.5194/essd-16-2099-2024, 2024.

Dietrich, G.: Die natürlichen Regionen von Nord- und Ostsee auf hydrographischer Grundlage, Kiel. Meeresforsch., 7, 35–69, 1950.

Dong, S., Volkov, D., Goni, G., Lumpkin, R., and Foltz, G. R.: Near-surface salinity and temperature structure observed with dual-sensor drifters in the subtropical S outh P acific, J. Geophys. Res. Oceans, 122, 5952–5969, https://doi.org/10.1002/2017JC012894, 2017.

Edson, J. B., Jampana, V., Weller, R. A., Bigorre, S. P., Plueddemann, A. J., Fairall, C. W., Miller, S. D., Mahrt, L., Vickers, D., and Hersbach, H.: On the Exchange of Momentum over the Open Ocean, J. Phys. Oceanogr., 43, 1589–1610, https://doi.org/10.1175/JPO-D-12-0173.1, 2013.

https://doi.org/10.5194/egusphere-2026-3332
Preprint. Discussion started: 24 June 2026

Fairall, C. W., Bradley, E. F., Godfrey, J. S., Wick, G. A., Edson, J. B., and Young, G. S.: Cool-skin and warm-layer effects on sea surface temperature, J. Geophys. Res. Oceans, 101, 1295–1308, https://doi.org/10.1029/95JC03190, 1996.

Fairall, C. W., Bradley, E. F., Hare, J. E., Grachev, A. A., and Edson, J. B.: Bulk Parameterization of Air–Sea Fluxes: Updates and Verification for the COARE Algorithm, J. Clim., 16, 571–591, https://doi.org/10.1175/1520-0442(2003)016<0571:BPOASF>2.0.CO;2, 2003.

Foroughan, M., Hamze-Ziabari, S. M., Lemmin, U., and Barry, D. A.: A Persistent Submesoscale Frontal Slick: A Novel Marker of the Mesoscale Flow Field in a Large Lake (Lake Geneva), Geophys. Res. Lett., 49, e2022GL100262, https://doi.org/10.1029/2022GL100262, 2022.

Gade, M., Hühnerfuss, H., and Korenowski, G. M.: Marine surface films: chemical characteristics, influence on air-sea interactions and remote sensing, Springer, Berlin, 2006.

Gallardo, C., Ory, N. C., Gallardo, M. D. L. Á., Ramos, M., Bravo, L., and Thiel, M.: Sea-Surface Slicks and Their Effect on the Concentration of Plastics and Zooplankton in the Coastal Waters of Rapa Nui (Easter Island), Front. Mar. Sci., 8, 688224, https://doi.org/10.3389/fmars.2021.688224, 2021.

Laxague, N. J. M., Zappa, C. J., Soumya, S., and Wurl, O.: The suppression of ocean waves by biogenic slicks, J. R. Soc. Interface, 21, 20240385, https://doi.org/10.1098/rsif.2024.0385, 2024.

Marmorino, G. O. and Smith, G. B.: Reduction of surface temperature in ocean slicks, Geophys. Res. Lett., 33, 2006GL026502, https://doi.org/10.1029/2006GL026502, 2006.

McDougall, T. J.: Small-scale turbulence and mixing in the ocean: A glossary, Elsevier Oceanogr. Ser, 46, 3–9, https://doi.org/10.1016/S0422-9894(08)70533-6, 1988.

McDougall, T. J. and Barker, P. M.: Getting Started with TEOS-10 and the Gibbs Seawater (GSW) Oceanographic Toolbox. SCOR/IAPSO WG127, ISBN 978-0-646-55621-5, 2011.

Meyerjürgens, J., Badewien, T. H., Garaba, S. P., Wolff, J.-O., and Zielinski, O.: A State-of-the-Art Compact Surface Drifter Reveals Pathways of Floating Marine Litter in the German Bight, Front. Mar. Sci., 6, 58, https://doi.org/10.3389/fmars.2019.00058, 2019.

Meyerjürgens, J., Ricker, M., Schakau, V., Badewien, T. H., and Stanev, E. V.: Relative Dispersion of Surface Drifters in the North Sea: The Effect of Tides on Mesoscale Diffusivity, J. Geophys. Res. Oceans, 125, e2019JC015925, https://doi.org/10.1029/2019JC015925, 2020.

Miracca Lage, M., Ménesguen, C., Schmitt, M., Umlauf, L., Merckelbach, L., and R. Carpenter, J.: Turbulence Observations and Energetics of Diurnal Warm Layers, , https://doi.org/10.5194/egusphere-egu25-1265, 2025.

Otto, L., Zimmerman, J. T. E., Furnes, G. K., Mork, M., Saetre, R., and Becker, G.: REVIEW OF THE PHYSICAL OCEANOGRAPHY OF THE NORTH SEA, Neth. J. Sea Res., 26, 161–238, https://doi.org/10.1016/0077-7579(90)90091-T, 1990.

Price, J. F., Weller, R. A., and Pinkel, R.: Diurnal cycling: Observations and models of the upper ocean response to diurnal heating, cooling, and wind mixing, J. Geophys. Res. Oceans, 91, 8411–8427, https://doi.org/10.1029/JC091iC07p08411, 1986.

https://doi.org/10.5194/egusphere-2026-3332
Preprint. Discussion started: 24 June 2026

Ricker, M., Meyerjürgens, J., Badewien, T. H., and Stanev, E. V.: Lagrangian Methods for Visualizing and Assessing Frontal Dynamics of Floating Marine Litter with a Focus on Tidal Basins, in: Chemical Oceanography of Frontal Zones, vol. 116, edited by: Belkin, I. M., Springer Berlin Heidelberg, Berlin, Heidelberg, 407–442, https://doi.org/10.1007/698_2021_812, 2021.

Schmitt, M., Pham, H. T., Sarkar, S., Klingbeil, K., and Umlauf, L.: Diurnal Warm Layers in the Ocean: Energetics, Nondimensional Scaling, and Parameterization, J. Phys. Oceanogr., 54, 2024.

Schmitt, R. W., Ledwell, J. R., Montgomery, E. T., Polzin, K. L., and Toole, J. M.: Enhanced Diapycnal Mixing by Salt Fingers in the Thermocline of the Tropical Atlantic, Science, 308, 685–688, https://doi.org/10.1126/science.1108678, 2005.

Soloviev, A. and Lukas, R.: Observation of large diurnal warming events in the near-surface layer of the western equatorial Pacific warm pool, Deep Sea Res. Part Oceanogr. Res. Pap., 44, 1055–1076, https://doi.org/10.1016/S0967-0637(96)00124-0, 1997.

St. Laurent, L. and Schmitt, R. W.: The Contribution of Salt Fingers to Vertical Mixing in the North Atlantic Tracer Release Experiment*, J. Phys. Oceanogr., 29, 1404–1424, https://doi.org/10.1175/1520-0485(1999)029<1404:TCOSFT>2.0.CO;2, 1999.

Turner, J. S.: Buoyancy effects in fluids, Cambridge University Press, 1973.

Umlauf, L., Burchard, H., and Bolding, K.: GOTM - Scientific Documentation Version 3.2, Mar. Sci. Rep., 63, 279 pp., https://doi.iow.de/10.12754/msr-2005-0063, 2005.

Watson, A. J., Bock, E. J., Jähne, B., Asher, W. E., Frew, N. M., Hasse, L., Korenowski, G. M., Merlivat, L., Phillips, L. F., Schluessel, P., Woolf, D. K., and Liss, P. S.: Report Group 1 – Physical processes in the microlayer and the air–sea exchange of trace gases, in: The Sea Surface and Global Change, edited by: Liss, P. S. and Duce, R. A., Cambridge University Press, 1–34, https://doi.org/10.1017/CBO9780511525025.002, 1997.

Watson, A. J., Schuster, U., Shutler, J. D., Holding, T., Ashton, I. G. C., Landschützer, P., Woolf, D. K., and Goddijn-Murphy, L.: Revised estimates of ocean-atmosphere CO2 flux are consistent with ocean carbon inventory, Nat. Commun., 11, 4422, https://doi.org/10.1038/s41467-020-18203-3, 2020.

Weiss, R. F.: Carbon dioxide in water and seawater: the solubility of a non-ideal gas, Mar. Chem., 2, 203–215, https://doi.org/10.1016/0304-4203(74)90015-2, 1974.

Witte, C. R. and Zappa, C. J.: The Response of Large Diurnal Warm Layers to Short-Term Variability in Solar and Wind Forcing: Observations and Physical Modeling, J. Phys. Oceanogr., 55, 2025.

Wurl, O., Stolle, C., Van Thuoc, C., The Thu, P., and Mari, X.: Biofilm-like properties of the sea surface and predicted effects on air–sea CO2 exchange, Prog. Oceanogr., 144, 15–24, https://doi.org/10.1016/j.pocean.2016.03.002, 2016.

Wurl, O., Bird, K., Cunliffe, M., Landing, W. M., Miller, U., Mustaffa, N. I. H., Ribas-Ribas, M., Witte, C., and Zappa, C. J.: Warming and Inhibition of Salinization at the Ocean's Surface by Cyanobacteria, Geophys. Res. Lett., 45, 4230–4237, https://doi.org/10.1029/2018GL077946, 2018.

https://doi.org/10.5194/egusphere-2026-3332
Preprint. Discussion started: 24 June 2026

Yan, Y., Song, X., Wang, G., and Li, X.: Tropical Cool-Skin and Warm-Layer Effects and Their Impact on Surface Heat Fluxes, J. Phys. Oceanogr., 54, 45–62, https://doi.org/10.1175/JPO-D-23-0103.1, 2024.

585 You, Y.: A global ocean climatological atlas of the Turner angle: implications for double-diffusion and water-mass structure, Deep Sea Res. Part Oceanogr. Res. Pap., 49, 2075–2093, https://doi.org/10.1016/S0967-0637(02)00099-7, 2002.